Contrib Mineral Petrol (2012) 163:1–17
DOI 10.1007/s00410-011-0655-y

ORIGINAL PAPER

Origin of Meso-Proterozoic post-collisional leucogranite suites (Kaokoveld, Namibia): constraints from geochronology and Nd, Sr, Hf, and Pb isotopes

S. Jung · K. Mezger · O. Nebel · E. Kooijman · J. Berndt · F. Hauff · C. Münker

Received: 8 December 2010 / Accepted: 23 May 2011 / Published online: 21 June 2011

Abstract Leucocratic granites of the Proterozoic Kaoko Belt, northern Namibia, now preserved as meta-granites, define a rock suite that is distinct from the surrounding granitoids based on their chemical and isotopic characteristics. Least evolved members of this ~1.5–1.6-Ga-old leucogranite suite can be distinguished from ordinary calc-alkaline granites that occur elsewhere in the Kaoko Belt by higher abundances of Zr, Y, and REE, more radiogenic initial ε_{Nd} values and unradiogenic initial $^{87}Sr/^{86}Sr$. The leucogranites have high calculated zircon saturation temperatures (mostly > 920°C for least fractionated samples), suggesting that they represent high-temperature melts originating from deep crustal levels. Isotope data (i.e., ε_{Ndi}: +2.3 to –4.2) demonstrate that the granites formed from different sources and differentiated by a variety of processes including partial melting of mantle-derived meta-igneous rocks followed by crystal fractionation and interaction with older crustal material. Most fractionation-corrected Nd model ages (T_{DM}) are between 1.7 and 1.8 Ga and only slightly older than the inferred intrusion age of ca. 1.6 Ga, indicating that the precursor rocks must have been dominated by juvenile material. Epsilon Hf values of zircon separated from two granite samples are positive (+11 and +13), and Hf model ages (1.5 and 1.6 Ga) are similar to the U–Pb zircon ages, again supporting the dominance of juvenile material. In contrast, the Hf model ages of the respective whole rock samples are 2.3 and 2.4 Ga, demonstrating the involvement of older material in the generation of the granites. The last major tectonothermal event in the Kaoko Belt in the Proterozoic occurred at ca. 2.0 Ga and led to reworking of mostly 2.6-Ga-old rocks. However, the presence of 1.6 Ga "post-collisional" granites reflects addition of some juvenile mantle-derived material after the last major tectonic event. The results suggest that similar A-type leucogranites are potentially more abundant in crustal terranes but are masked by AFC processes. In the case of the Kaoko Belt, it is suggested that this rock suite indicates a yet unidentified period of mantle-derived crustal growth in the Proterozoic of South Western Africa.

Keywords Leucogranite · U–Pb geochronology · Sr–Nd–Pb–Hf isotopes · Kaoko Belt · Namibia

Communicated by J. Hoefs.

Electronic supplementary material The online version of this article (doi:10.1007/s00410-011-0655-y) contains supplementary material, which is available to authorized users.

S. Jung (✉)
Department Geowissenschaften, Institut für Mineralogie und Petrographie, Universität Hamburg, Grindelallee 48, 20146 Hamburg, Germany
e-mail: stefan.jung@mineralogie.uni-hamburg.de

K. Mezger
Institut für Geologie, Universität Bern, Baltzerstrasse 1+3, 3012 Bern, Switzerland

O. Nebel
Research School of Earth Sciences, The Australian National University, Canberra, ACT 0200, Australia

E. Kooijman · J. Berndt
Universität Münster, Institut für Mineralogie, Corrensstraße 24, 48149 Münster, Germany

F. Hauff
IFM-GEOMAR, Research Division 4, Dynamics of the Ocean Floor, Wischhofstrasse 1-3, 24148 Kiel, Germany

C. Münker
Institut für Geologie und Mineralogie, Universität zu Köln, Zülpicherstr. 49b, 50674 Köln, Germany

Introduction

Igneous rocks are indispensable sources of information for the reconstruction of the evolution of orogenic belts. Their age relations and elemental and isotopic compositions provide evidence for the identity of unexposed basement terranes (Bennett and DePaolo 1987; Ayuso and Bevier 1991; Dorais and Paige 2000). In areas such as the Kaoko Belt, Namibia, where country rock gneisses (as potential end member source compositions of granitoids) may bear considerable similarity to one another, detailed studies of individual precisely dated meta-igneous complexes are necessary to quantify their petrogenesis and tectonic position within the orogen (Kröner et al. 2004; Konopásek et al. 2005; Luft et al. 2011). The main exposed basement sources in the Kaoko Belt are Archaen to Proterozoic granodioritic to granitic gneisses that have distinct Nd isotope signatures (Seth et al. 1998). However, the composition and evolution of the basement underlying the Kaoko Belt is likely to be very complex, requiring assessment of additional source components, including various mantle reservoirs and mid-crustal metasedimentary and meta-igneous rocks. In this context, geochemical tracers, particularly isotope systems, yield important petrogenetic information. This study is focused on a particular suite of leucogranites that occurs within strongly deformed metapelitic to meta-igneous country rock gneisses. These leucogranites have clear intrusive relationships with the country rock gneisses and are more massive and less deformed than the rocks into which they intruded although all rock types have undergone at least two episodes of high-grade deformation and metamorphism. Previous studies (e.g., Kröner et al. 2004) have shown that Pan-African intrusive rocks are absent in the area and a likely age for the country rock gneisses is 2.0 Ga. Hence; identifying and quantifying distinct mantle or crustal source components for the leucogranites will lead to better-constrained tectonic models for their genesis.

The Mid-Proterozoic central part of the Kaoko Belt (CKZ; Central Kaoko Zone of Seth et al. 1998; Goscombe et al. 2003; Kröner et al. 2004) is the least well-understood part of the orogen. Here and elsewhere in the orogen, isolated leucogranite bodies are exposed. Generally, leucogranites are a small but genetically important component of granitic intrusions in most orogenic belts. Their petrogenesis and tectonic significance has been the focus of much discussion (e.g., Dietrich and Gansser 1981; Vidal et al. 1982; Bernard-Griffiths et al. 1985; LeFort et al. 1987; Deniel et al. 1987; France-Lanord and Le Fort 1988; Ortega and Gil-Ibarguchi 1990; Scaillet et al. 1990; Inger and Harris 1993; Searle et al. 1997).

Most leucogranites are peraluminous and are considered to represent pure crustal melts; a conclusion supported by (1) similar isotope signatures of leucogranites and associated metasedimentary rocks, (2) their common field setting within high-grade regional metamorphic terranes, (3) a lack of spatial and temporal associations between them and basaltic magmatism and (4) experimental studies using natural pelitic compositions. The classical model for the generation of this type of leucogranite involves melting aided by fluxing of fluids derived from dehydration of metasedimentary rocks during "hot-over-cold" thrusting of crustal slices during orogeny (LeFort et al. 1987). Other leucogranites may have been derived by extensive fractional crystallization from more intermediate parent magmas that have an input from the upper mantle (Crawford and Windley 1990; Searle et al. 1992). Thus, at least two different processes have been identified, often within the same collisional environment.

Here we evaluate the significance of c. 1.6-Ga-old highly fractionated leucogranites in the Kaoko Belt of Namibia. In order to constrain the nature of felsic magmatism, major and trace element and Sr, Nd, Hf, and Pb isotope data (the latter obtained on acid-leached K-feldspar separates) are presented. Collectively, the results are used to constrain the petrogenesis of the leucogranites and have implications for melt generation and modification in high-grade terranes. Singling out which processes and sources were involved in the petrogenesis of these leucogranites is a fundamental step in furthering the understanding of granite petrogenesis.

Geological setting

The Kaoko Belt is the NNW-trending northern arm of the Neoproterozoic Damara Orogen extending c. 700 km from the Ugab Zone in the south to Angola in the north (Fig. 1). The equivalents to the western margin of the Kaoko Belt in Brazil are the Dom Feliciano and Ribeira Belts flanking the Rio de la Plata Craton (Porada 1989; Trompette and Carozzi 1994). In the Kaoko Belt, a mosaic of Archaen, Palaeoproterozoic and Mesoproterozoic metamorphic and igneous basement complexes, which form the SW margin of the otherwise predominantly Archaen Congo Craton, is unconformably overlain by the Neoproterozoic Damara Sequence. Deposition of the Damara Sequence was terminated by collision in the late Neoproterozoic and was followed by a protracted tectonothermal evolution collectively called the Damara Orogeny, which occurred from the late Neoproterozoic to Cambrian time (Miller 1983, 2008; Prave 1996).

The Kaoko Belt sensu stricto is subdivided into three NNW-trending parallel zones (Eastern Kaoko Zone (EKZ), Central Kaoko Zone (CKZ), and Western Kaoko Zone (WKZ)) of characteristic tectonic and metamorphic style (Miller 1983; Goscombe et al. 2003). Additionally, two

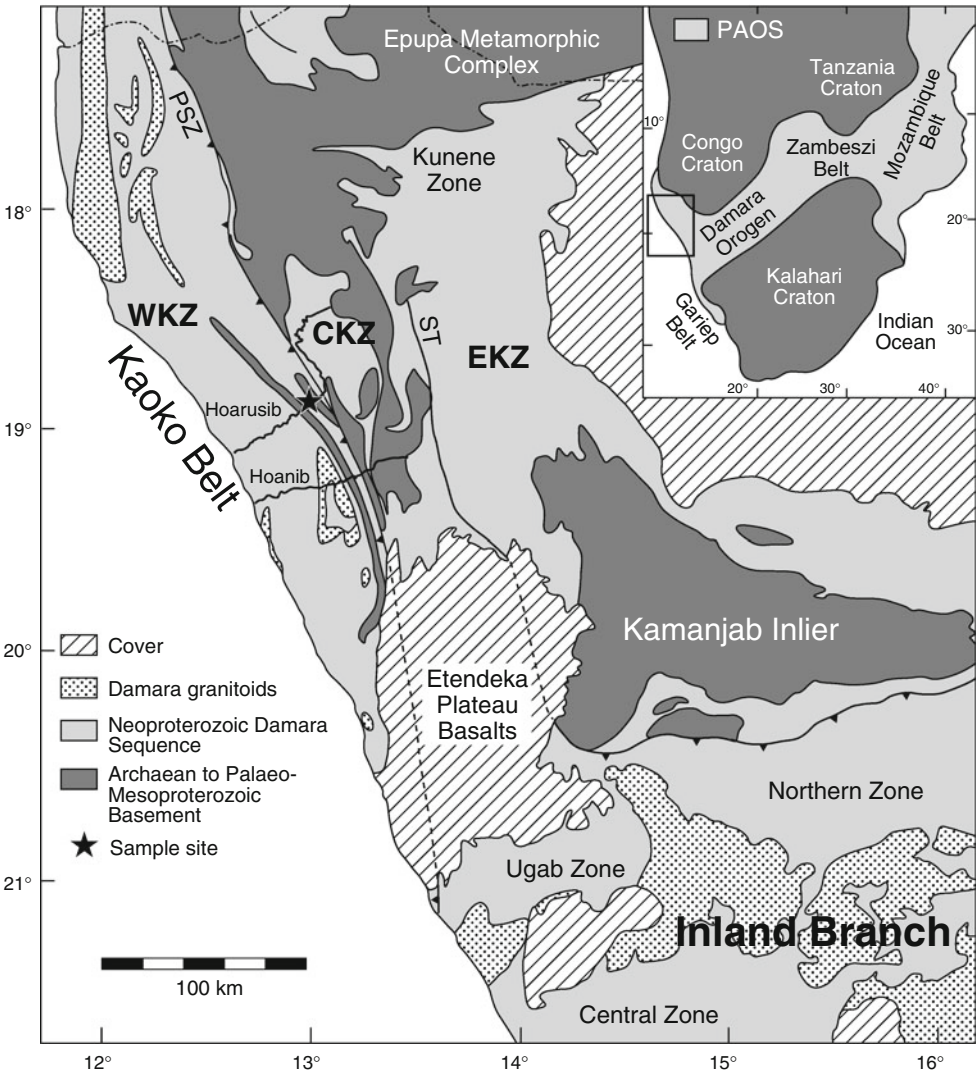

Fig. 1 Generalized geological map of the Kaoko Belt (Namibia) modified by Goscombe et al. (2003). *Inset* shows the position of the Kaoko Belt relative to the Archaen to Proterozoic Congo and Kalahari cratons. *EKZ* Eastern Kaoko Zone, *CKZ* Central Kaoko Zone, *WKZ* Western Kaoko Zone, *ST* Sesfontein Thrust, *PSZ* Puros Shear Zone, *PAOS* Pan-African Orogenic System. *Star* denotes sample site in the upper reaches of the Hoarusib River, and GPS data for the sample locations are given in Table 1

other zones are distinguished at each end of the belt, the Kunene Zone in the north and the Ugab Zone in the south (Fig. 1). The Eastern Kaoko Zone (EKZ) consists of sub-greenschist facies platform carbonates deformed by east–west shortening during Pan-African times. Its western margin is marked by the shallow west-dipping Sesfontein Thrust, which formed under brittle conditions late in the Damara orogenic cycle (Dürr and Dingeldey 1996). The Central Kaoko Zone (CKZ) ranges from lower-greenschist in the east to upper-amphibolite facies in the west. The western margin of the CKZ is delineated by the Puros Mylonite Zone (PMZ) which is a prominent shear zone running along the entire length of the Kaoko Belt. The Western Kaoko Zone (WKZ) is a core complex composed of shear zone bounded areas of amphibolite to granulite facies members of the Damara Sequence with a high proportion of partial melts and Neoproterozoic granitoids. Within the Western Kaoko Zone, the Village Mylonite Zone, which runs c. 100 km through the WKZ, separates a Mesoproterozoic part in the east from a Neoproterozoic part in the west. The Kunene Zone in the NE Kaoko Belt is dominated by Pre-Pan-African basement rocks associated with low-grade sedimentary rocks of the Damara Sequence (Brandt et al. 2007; Drüppel et al. 2007). The Ugab Zone in the south consists of greenschist facies, turbiditic Damara Sequence rocks that have been pervasively deformed by very tight folding without involvement of the basement (Passchier et al. 2002). Intrusions are restricted to syn-orogenic syenites and granites (Seth et al. 2000; Jung et al. 2005).

The geochronology for the different tectonic domains that constitute the composite Damara-Kaoko orogenic system is fairly well constrained. U–Pb zircon ages of 2.65–2.58 Ga for granulite facies gneisses along the Hoanib Valley (Fig. 1, Seth et al. 1998) date the oldest rocks so far known in Namibia. Some samples yielded Palaeo-Proterozoic ages ranging from 1.99 to 1.96 Ga. Recently, Kröner et al. (2004) investigated the basement

rocks along a traverse in the Hoarusib Valley (Fig. 1). They obtained U–Pb SHRIMP and conventional U–Pb zircon ages that range from 2.20 Ga to 1.68 Ga but also from 1.52 to 1.45 Ga. Additionally, U–Pb SHRIMP, Pb–Pb evaporation, and conventional U–Pb ages for metamorphic and igneous zircon are c. 730, 700, 650, and c. 550 Ma, respectively. These ages agree with the results obtained by Seth et al. (1998) and Franz et al. (1999) who postulated two distinct episodes of Pan-African metamorphism due to the occurrence of c. 650- and c. 560-Ma-old monazite and zircon in granitoid gneisses. The younger monazite ages agree with a Sm–Nd garnet age of c. 570 Ma presented by Goscombe et al. (2003) which was interpreted to reflect the time of high-grade metamorphism in the area. The significance of the 650 Ma age was recently confirmed by Seth et al. (2008) by dating metamorphic minerals such as kyanite and garnet with different techniques (Sm–Nd, Lu–Hf, Pb–Pb).

Description of the granites and their country rocks

The Mesoproterozoic part of the Kaoko Belt represented by the Western Kaoko Zone (WKZ) east of the Puros Shear Zone (PSZ) was metamorphosed under uniformly high-grade conditions that range from upper amphibolite to lower granulite facies and shows complex structures typical of many granite-migmatite terranes. In this study, we investigate the relationships between leucogranites (now preserved as partly recrystallized orthogneisses) and migmatized country rock gneisses. In addition, we compare the leucogranites with 1.5-Ga-old granite gneisses of uncertain origin from the terrane (Kröner et al. 2004) and also from the nearby Hoanib River (Luft et al. 2011) because of their similar age. To derive at a broader picture, we also compare the country rock gneisses with Archaen to Proterozoic gneisses from elsewhere in the Kaoko Belt, because these gneisses may be, in general, potential source rocks of the granites or potential end members in assimilation-fractional crystallization scenarios.

The country rocks collected in the vicinity of the leucogranites are mostly migmatitic meta-igneous and metasedimentary gneisses, showing continuous banding on the millimeter to centimeter scale which is defined by alternating, well-foliated biotite and amphibole-rich layers and granular quartz-feldspar layers. Within the migmatitic gneisses, a pre-migmatisation fabric (e.g., layering and foliation) is well developed within the paleosome although the neosome-paleosome ratio may be variable. Migmatitic gneisses show diffuse and irregular borders toward the leucogranites. In the field, the dominant type of leucogranite is a white to pinkish, medium-grained biotite-bearing granite with rare garnet showing abundant mafic schlieren toward the country rocks. The leucogranite sheets are numerous within the country rock gneisses (c. 10–20) and range in thickness from 20 to 30 cm to 1–2 m. For the small-sized sheets, it is difficult to evaluate whether their thickness was reduced due to metamorphic compression, but the larger sheets appear to be massive without any signs of volume reduction. In the sample area, the sheets are evenly distributed within the country rock gneisses, but there are also country rock gneisses without granite intrusions.

The most common mineral assemblage in pelitic gneisses is biotite–plagioclase–K-feldspar–quartz ± sillimanite ± garnet with minor secondary muscovite and accessory tourmaline, apatite, zircon, monazite, and Fe–Ti oxides. Cordierite was not observed, mainly because the bulk composition of the metapelitic country rock gneisses was unsuitable to form cordierite. The observed parageneses are in accordance with the regional distribution of metamorphic isograds presented by Will et al. (2004) which indicate that the sample site lies above the grt-crd-sil-kfs isograd. In meta-igneous gneisses, plagioclase + biotite + hornblende + quartz ± K-feldspar are the major rock-forming minerals with accessory allanite, apatite, zircon, and Fe–Ti oxides. Quartz, perthitic alkali feldspar, and plagioclase make up to 90 vol% in the leucogranite, but proportions of alkali feldspar to plagioclase are variable. Large K-feldspar crystals may be phenocrystic, but some of them show signs of recrystallization as a result of metamorphic overprint in Pan-African times. Biotite in the leucogranite occurs either as mineral aggregates or as individual crystals. Garnet forms anhedral, inclusion-poor crystals with prominent quartz and plagioclase moats or embayed crystals with inclusions of biotite and quartz. Typical accessory phases within the garnet-bearing leucogranite include zircon, allanite, and apatite in decreasing order of abundance.

Geochronology

To constrain the likely intrusion age of the granites, several zircon fractions from sample A4 and A5 were analyzed for U and Pb isotopes by LA-ICP-MS. Procedures are outlined in the Online Resource 1, and data and figures are given in the Online Resource 2 and 3. The zircon population is very similar in both samples and consists of euhedral pinkish grains with rounded terminations. The zircons are 100–300 μm long with a length/width ratio of 2–4, suggesting an originally magmatic origin for these grains (Pupin 1980). All selected fractions were free of visible inclusions.

Both samples yield maximum ages of 1.5–1.6 Ga. These upper intercept ages are interpreted to represent the intrusion age of the granites. They may have geological significance since similar U–Pb zircon ages between

1,448 ± 31 and 1,516 ± 54 Ma have been reported by Kröner et al. (2004) for this part of the Kaoko Belt, and Seth et al. (1998) reported an age of 1,507 ± 16 Ma for an orthogneiss from the nearby Hoanib River. In addition, Luft et al. (2011) reported U–Pb zircon ages of 1,506 ± 19 Ma and 1,503 ± 12 Ma for leucogranites from the Hoanib River. Similarly, Rb–Sr whole rock systematics from the granites also point to an age of ca. 1.6 Ga (Online Resource 4). Lower concordia intercept ages are around 550 and 580 Ma and have geological meaning because they are similar to the oldest U–Pb monazite ages of about 580 Ma from the Kaoko Belt, which are interpreted to represent the age of peak metamorphism (Jung et al. unpublished). It is interesting to note that the early Pan-African metamorphic (Franz et al. 1999) and magmatic event with an approximate age of ca. 650 Ma (Seth et al. 1998, 2008) had obviously no imprint on the U–Pb systematics of the zircons investigated here.

Geochemistry

The SiO_2 contents of the leucogranites range from 72 to 77 wt% (Online Resource 5). They are metaluminous to peraluminous with alumina saturation indices (ASI) (ASI: molar A/CNK: $(Al_2O_3/CaO + Na_2O + K_2O)$) between 0.95 and 1.14. Significant features are $K_2O > Na_2O$ and a strong variation in Na_2O and CaO contents (Fig. 2). Rubidium and Ba are enriched relative to Sr (Fig. 3), and therefore, Rb/Ba and Rb/Sr ratios are high, but Sr/Ba ratios are low. K/Rb ratios range from 140 to 320. Based on their REE contents, the leucogranites can be subdivided into two groups. Group I is LREE- and HREE-enriched with chondrite-normalized La abundances from ca. 260 to 320 and moderately negative Eu anomalies (Eu/Eu*: 0.54–0.41; samples A9A, A9B, A4A, A4B, A7; Fig. 4a). Chondrite-normalized La_n/Yb_n ratios range from 5.9 to 7.3. These features suggest that this group comprises the least evolved samples. Group II leucogranites (Fig. 4b; samples A8 and A11) are characterized by higher LREE and HREE contents but similar chondrite-normalized La_n/Yb_n ratios. Additionally, a strong negative Eu anomaly (Eu/Eu*: 0.12) is present. These leucogranites are enriched in Rb, Th and U and depleted in Sr, Ba, MgO, and P_2O_5 relative to Group I leucogranites. Hence, they have higher Rb/Sr but also higher Rb/Ba and Sr/Ba ratios than the Group I leucogranites. Therefore, Group II leucogranites can be regarded as more fractionated. Due to similar Rb/Sr, Rb/Ba, and Sr/Ba ratios, sample A5 that is characterized by lower LREE contents and a wing-shaped REE pattern (Fig. 4b) with strong HREE enrichment may belong to Group I leucogranites.

The partly migmatized country rocks are Fe-rich but Mg- and Ti-poor gneisses with $K_2O \geq Na_2O$, moderate Al_2O_3 but high CaO (Fig. 2, Online Resource 5), high Ba, Sr, Zr (Fig. 3) and high REE concentrations (Fig. 4c) together with highly variable negative Eu anomalies (Eu/Eu*: 0.84–0.35). Alumina saturation indices are mostly below 1. Therefore, these gneisses are classified as meta-igneous gneisses, a conclusion also supported by their P_2O_5/TiO_2 versus MgO/CaO relationships (Fig. 2; Werner 1987).

Nd, Sr, Pb and Hf Isotopes

The results of the Sr, Nd, and Pb isotope analyses are reported in Table 1, and Hf isotope data for zircon and whole rocks are given in Table 2. Analytical details are

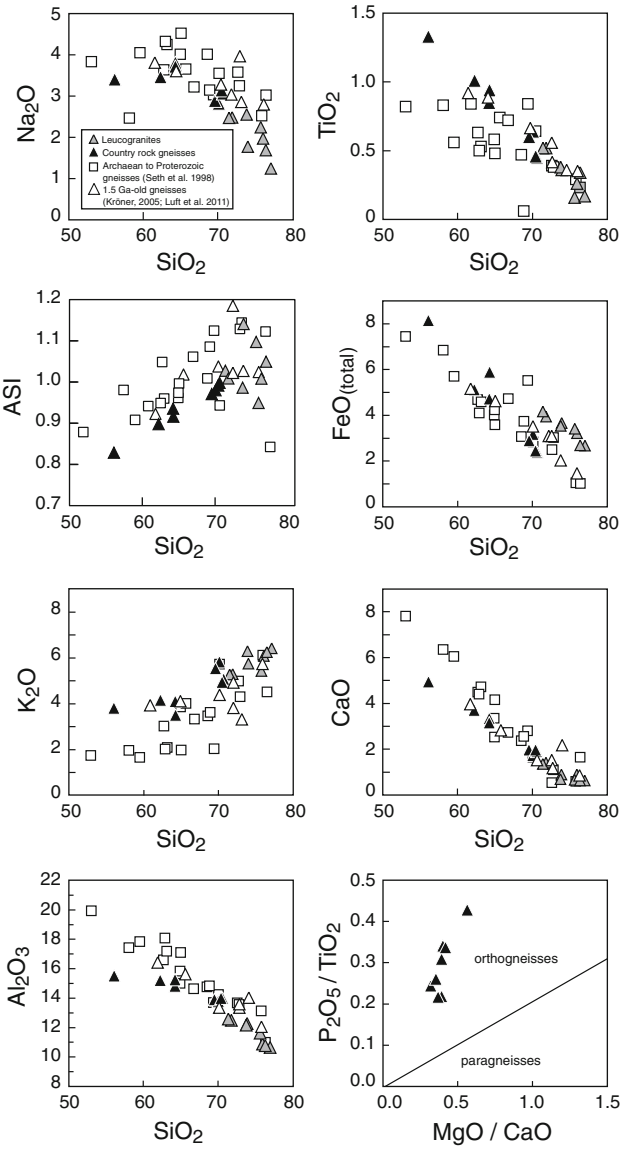

Fig. 2 Major element plots for leucogranites, country rocks, and basement gneisses

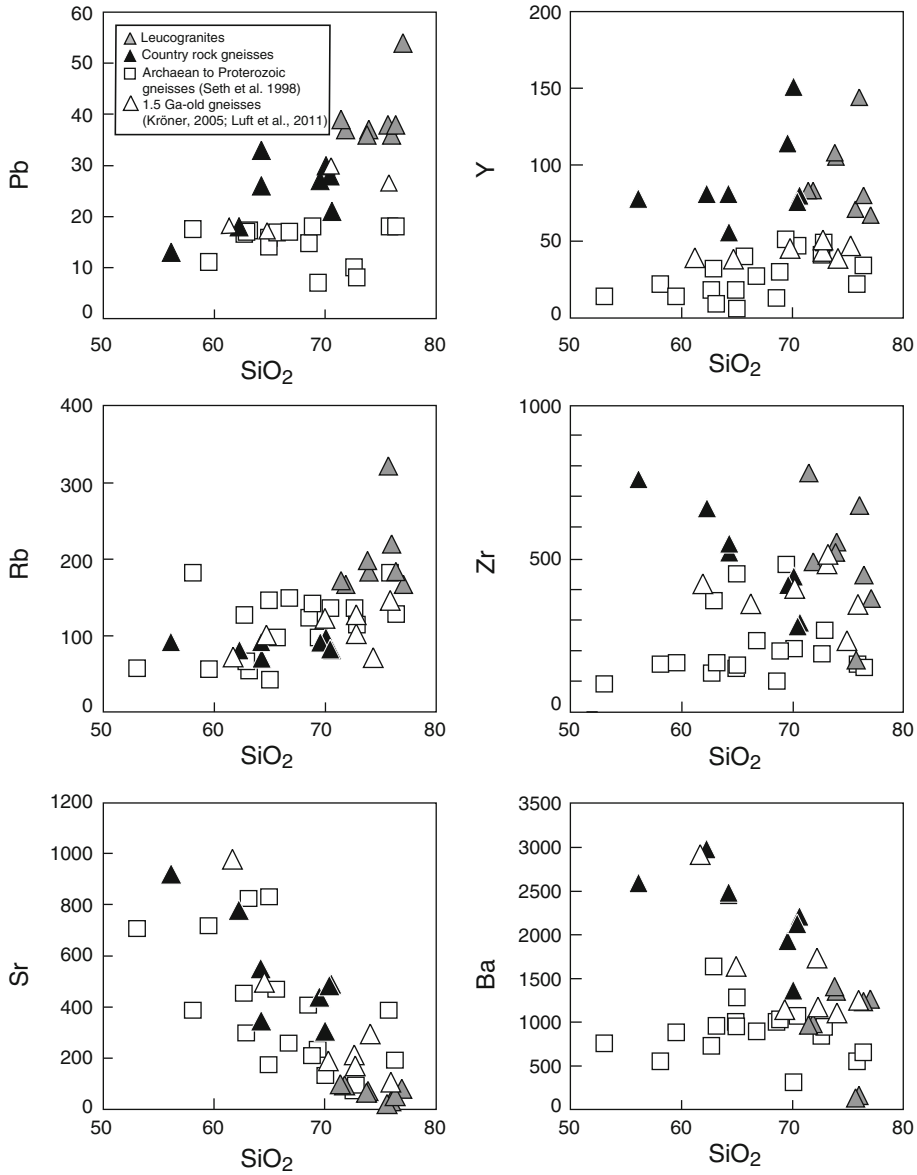

Fig. 3 Selected trace element plots for leucogranites, country rocks, and basement gneisses

given in the Online Resource 1. The leucogranites have initial ε_{Nd} values (at 1,600 Ma) from +2.3 to −4.6 and initial $^{87}Sr/^{86}Sr_{(1,600\ Ma)}$ ratios from 0.70298 to 0.71594 (Fig. 5a). In a $^{87}Rb/^{86}Sr$ isochron plot (Online Resource 4), the leucogranites studied here as well as the samples studied by Kröner (2005) where Sr isotopes were determined during this study and the samples studied by Luft et al. (2011) plot along a reference line corresponding to an age of c. 1.6 Ga. This age is roughly the same as the U–Pb zircon ages (Online Resource 3) The variable $^{147}Sm/^{144}Nd$ ratios are in many samples higher than the average continental crust (0.114; Rudnick and Fountain 1995) and were likely modified during the petrogenesis of the leucogranites. Therefore, depleted mantle Nd model ages are calculated following the procedure outlined by Millisenda et al. (1994) and are mostly between 1.7 and 1.9 Ga. One sample (A5) has a slightly higher Nd model age of 2.2 Ga. The $^{206}Pb/^{204}Pb$ and $^{207}Pb/^{204}Pb$ ratios obtained on acid-leached K-feldspar for the leucogranites range from 18.35 to 20.02 and 15.67 to 15.80, respectively; the $^{208}Pb/^{204}Pb$ ratios range from 38.00 to 40.07. The leucogranites plot above and/or to the right of the two-stage U–Pb growth curve defined by Stacey and Kramers (1975). In $^{208}Pb/^{204}Pb$ vs. $^{206}Pb/^{204}Pb$, the samples straddle along the growth curve defined by Stacey and Kramers (1975) (Fig. 6a and b). The country rock gneisses have initial ε_{Nd} values (at 1,600 Ma) between −1.4 and −6.7 and initial $^{87}Sr/^{86}Sr_{(1,600\ Ma)}$ ratios between 0.70167 and 0.70342 (Fig. 5). Although there is some overlap with the Pb isotope ratio obtained on the leucogranites, the $^{206}Pb/^{204}Pb$ and $^{207}Pb/^{204}Pb$ ratios of acid-leached K-feldspar from the gneisses appear to be less radiogenic and range from 17.48

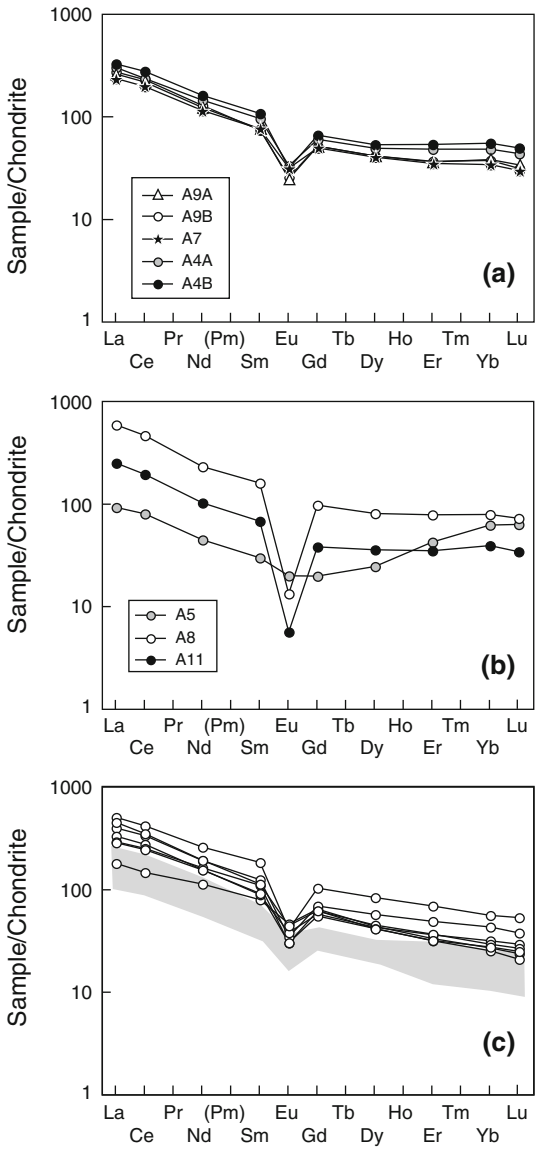

Fig. 4 Chondrite-normalized rare earth element plots for **a** unfractionated leucogranites, **b** fractionated leucogranites, and **c** country rock gneisses. *Shaded area* in (**c**) represents four analyses of 1.5-Ga-old gneisses from Kröner (2005) and three analyses of 1.5-Ga-old gneisses from Luft et al. (2011). Normalization factors according to Boynton (1984). Note that the inferred unfractionated leucogranites are REE-enriched with mildly developed negative Eu anomalies. More fractionated leucogranites have elevated REE abundances and strongly negative Eu anomalies either due to the removal of feldspar or depleted REE compositions due to the fractionation of REE-enriched accessory mineral phases. The *wing-shaped* REE pattern of sample A5 is the result of accumulation of garnet

to 18.81 and 15.54 to 15.71, respectively; the $^{208}Pb/^{204}Pb$ ratios range from 36.98 to 38.80 (Fig. 6). Lutetium and Hf concentration data and Hf isotope data for zircon from samples A5 and A4 and for the leucogranites are presented in Table 2. For zircon, moderately high Lu but extremely high Hf concentrations in zircon result in very low $^{176}Lu/^{177}Hf$ ratios and unradiogenic initial $^{176}Hf/^{177}Hf$ ratios. Initial Hf isotope data, expressed as initial ε_{Hf} values, are strongly positive (+11.0 and +12.9). Depleted mantle Hf model ages are 1.5 and 1.6 Ga for the two zircon separates, essentially the same as the U–Pb zircon ages. The whole rock samples have moderately high Lu and Hf concentrations and moderately low $^{176}Lu/^{177}Hf$ ratios. Their initial $^{176}Hf/^{177}Hf$ ratios expressed as initial ε_{Hf} values are fairly primitive (−0.64 to +8.84) and their depleted mantle Hf model ages range from 1.7 to 2.4 Ga.

Discussion

The role of fractional crystallization and AFC processes

The chemical variation among the granites, albeit limited, can be interpreted as a result of fractional crystallization. Negative trends of TiO_2, MgO, FeO, CaO, and Al_2O_3 versus SiO_2 (Fig. 2) suggest minor fractionation of biotite but significant fractionation of K-feldspar and/or plagioclase. Increasing REE contents with an accompanying increase of the negative Eu anomaly indicate fractionation of plagioclase and K-feldspar and no significant fractionation of REE-enriched accessory phases, i.e., monazite or allanite in the early stages of differentiation. However, late-stage samples have lower LREE abundances, indicating that fractionation of LREE-enriched accessory phases became important. The effect of crystal fractionation processes is best illustrated in bivariate element-element plots that use elements (e.g., Rb, Sr) with a high distribution coefficient (Kd) for feldspars. Figure 7 is an evaluation of the most likely fractionating mineral assemblage that affects Rb and Sr concentrations. It is evident that the negative correlation between Rb and Sr can be satisfactorily accounted for by 50% crystallization of a 1:1 mixture of K-feldspar and plagioclase. The most fractionated sample record roughly 70% fractional crystallization. This is also consistent with the size of the negative Eu anomaly that correlates with Sr and Rb concentrations.

Strontium and Nd isotope compositions are heterogeneous which preclude a single homogeneous source for the origin of the granites. Initial $^{87}Sr/^{86}Sr$ ratios and ε_{Nd} values do not correlate with major or trace element abundances. This again implies a heterogeneous source and/or the primary melt was modified by AFC processes. Negative correlations in Nd–Sr space observed in granites (e.g., Halliday et al. 1980; DePaolo 1981a, b; McCulloch and Chappell 1982; Ben Othman et al. 1984; Pickett and Wasserburg 1989) are commonly attributed to a two-component mixing model where melts from the upper mantle with less negative or even positive ε_{Nd} values and unradiogenic Sr isotope compositions mix with upper or

Table. 1 Isotope composition of country rock gneisses and granites (Central Kaoko Zone, Kaokoveld, Namibia)

Sample	A1	A10	A16	A17	A18A	A9A	A9B	A8	A4A	A4B	A5	A7	Na 00-07	Na 00-10	Na 00-28	Na 00-23
$^{87}Sr/^{86}Sr(m)$	0.716917	0.708321	0.716687	0.713246	0.714076	0.828383	0.826593	1.203655	0.872026	0.905649	0.844107	0.949376	0.715413	0.706914	0.812155	0.746063
Error	0.000014	0.000012	0.000013	0.000011	0.000015	0.000010	0.000013	0.000012	0.000016	0.000011	0.000013	0.000015	0.000006	0.000005	0.000005	0.000006
$^{87}Sr/^{86}Sr(i)$	0.703420	0.701669	0.702930	0.702139	0.703102	0.710227	0.709846	0.715938	0.702988	0.703059	0.705274	0.709430	0.703044	0.702526	0.710641	0.706506
$^{87}Rb/^{86}Sr$	0.5837	0.2895	0.5987	0.4833	0.4775	5.142	5.097	21.223	7.356	8.816	6.041	10.441	0.569	0.203	4.665	1.904
$^{143}Nd/^{144}Nd(m)$	0.511740	0.511743	0.511766	0.511721	0.511801	0.511913	0.511926	0.512068	0.511874	0.511887	0.511887	0.511777	0.511905	0.511752	0.511660	0.511695	0.511788
Error	0.000013	0.000012	0.000015	0.000010	0.000011	0.000016	0.000017	0.000012	0.000014	0.000012	0.000015	0.000016	0.000015	0.000012	0.000011	0.000010
ε Nd (today)	−17.5	−17.5	−17.0	−17.9	−16.3	−14.1	−13.9	−11.1	−14.9	−14.6	−16.8	−14.3	−17.3	−19.1	−18.4	−16.6
$^{147}Sm/^{144}Nd$	0.1234	0.1382	0.1278	0.1167	0.1327	0.1266	0.1132	0.1416	0.1168	0.1148	0.1565	0.1295	0.1035	0.1023	0.1183	0.1092
$^{143}Nd/^{144}Nd(i)$	0.510495	0.510228	0.510365	0.510493	0.510346	0.510581	0.510685	0.510579	0.510645	0.510679	0.510335	0.510485	0.510723	0.510650	0.510516	0.510749
ε Nd (i)	−1.4	−6.7	−4.0	−1.5	−4.4	+0.2	+2.3	+0.2	+1.5	+2.2	−4.6	−1.7	+0.8	−0.9	−3.2	−0.34
f (Sm/Nd)	−0.37	−0.27	−0.32	−0.41	−0.30	−0.36	−0.40	−0.28	−0.41	−0.42	−0.30	−0.31	−0.47	−0.48	−0.39	−0.44
T DM	2.1	2.7	2.3	2.0	2.4	1.9	1.7	1.9	1.8	1.7	2.2	2.1	1.8	1.9	2.1	1.8
Sm	10.94	15.64	24.46	17.48	21.62	14.63	14.33	30.85	17.84	18.23	6.254	14.63	9.3	10.5	6.8	12.8
Nd	55.88	68.44	115.8	94.38	98.52	72.84	76.57	137.34	92.35	96.03	24.16	68.28	54.1	61.8	34.6	70.6
Rb	70	92	91	92	81	167	172	220	183	198	167	184	97	72	144	130
Sr	345	920	440	551	491	94	98	30	72	65	80	51	469	974	85	188
$^{206}Pb/^{204}Pb$	17.484	17.639	18.554	18.813	18.513	18.535	n.d.	18.350	18.414	n.d.	20.015	19.377	n.d.	n.d.	n.d.	n.d.
$^{207}Pb/^{204}Pb$	15.548	15.567	15.669	15.706	15.670	15.681	n.d.	15.669	15.677	n.d.	15.838	15.766	n.d.	n.d.	n.d.	n.d.
$^{208}Pb/^{204}Pb$	36.981	37.395	38.488	38.797	38.489	38.553	n.d.	38.395	38.001	n.d.	40.070	39.299	n.d.	n.d.	n.d.	n.d.

Uncertainties in the $^{87}Sr/^{86}Sr$ and $^{143}Nd/^{144}Nd$ ratios are 2 σ (mean) errors in the last two digits. ε Nd values are calculated relative to CHUR according to Jacobsen and Wasserburg (1980). Depleted mantle Nd model ages (T DM) are calculated according to Michard et al. (1985). For samples with $147Sm/144Nd > 0.12$, the correction procedure from Millisenda et al. (1994) was applied. *m* measured, *i* initial calculated for an age of 1.6 Ga. Samples Na 00-07 to Na 00-23 are from the study by Kröner (2005). Sr isotopes of these samples are from this study

lower crustal rocks with more negative ε_{Nd} values and radiogenic Sr isotope compositions. The c. 1.6-Ga-old granites from the Kaokoveld do not follow such a simple covariant array (Fig. 5a). Therefore, simple mixing relationships between mantle-derived melts and crustal rocks seems unlikely since none of the evolved samples fall directly in the field of known lower crustal lithologies from the Kaokoveld and more complex, two-stage or multi-stage AFC processes may have been operative. Overall, the granites have distinct isotope compositions. Three samples have positive ε_{Nd} values and a range of initial $^{87}Sr/^{86}Sr$ ratios although the high $^{87}Rb/^{86}Sr$ ratios preclude a detailed evaluation. Other samples evolved toward more radiogenic Sr isotope compositions at slightly positive ε_{Nd} values. Another subset of samples has unradiogenic Sr isotope compositions and negative ε_{Nd} values. The country rock gneisses have also unusual isotope compositions relative to known 2.6–2.0-Ga-old gneisses from the area (Seth et al. 2002) because of their unradiogenic $^{87}Sr/^{86}Sr$ ratios accompanied by only moderately negative ε_{Nd} values (Fig. 5).

Processes of assimilation of pre-existing crustal rocks by intruding magmas are best illustrated using isotope systems with different properties (i.e., Sr, Nd). Figure 5 shows two possible AFC curves using the most extreme crustal end member from the Kaokoveld and it can be seen that the curved array approximates the evolution of the samples that show increasing $^{87}Sr/^{86}Sr$ ratios, but virtually unchanged ε_{Nd} is best modeled with an orthogneiss from the 2.6-Ga-old basement as the contaminant. The model that older crustal material must have been involved is also supported by the high $^{207}Pb/^{204}Pb$ and $^{206}Pb/^{204}Pb$ ratios of the two samples with the most negative ε_{Nd} values. The samples that have less radiogenic $^{87}Sr/^{86}Sr$ ratios cannot be explained in this way. The Sr isotope composition of these samples requires contaminants with less radiogenic $^{87}Sr/^{86}Sr$. Epsilon Hf values of the leucogranites range from +8.8 to −0.7, in accordance with their Nd isotope composition. However, most Hf model ages are significantly older than their inferred emplacement ages indicating the presence of an older component in the evolution of these samples. Lead isotopes can also be used to constrain possible contaminants in the evolution of these granites. As shown in Fig. 6, Pb isotope compositions of the leucogranites plot onto or above and/or to the left of the two-stage Pb evolution curve defined by Stacey and Kramers (1975). To move the best fit straight line drawn through the feldspar data to a $^{206}Pb/^{204}Pb$–$^{207}Pb/^{204}Pb$ point corresponding to an age of 1.6 Ga (the likely intrusion age), the second-stage μ value must be adjusted to 10.08; a value slightly higher than the second stage μ value of 9.73 according to Stacey and Kramers (1975). The inferred contaminant must have higher $^{207}Pb/^{204}Pb$ and $^{206}Pb/^{204}Pb$ ratios. Although

Table 2 Lutetium and Hf abundances and Lu/Hf isotope systematics of leucogranites (WR = whole rock) and zircon from two samples

Sample name	A5 Zrc	A4 Zrc	A5-WR	A4B-WR	A7-WR	A8-WR	A9A-WR	A4A-WR	A9B-WR
ppm Lu	24.355	26.967	1.920	1.868	1.289	2.306	1.171	1.39	1.146
ppm Hf	10867	12338	15.80	15.37	12.92	29.33	14.03	11.37	14.05
$^{176}Lu/^{177}Hf$	0.000307	0.000300	0.01725	0.01725	0.01415	0.01116	0.01185	0.01702	0.01158
$^{176}Hf/^{177}Hf$	0.282087	0.282140	0.282271	0.282336	0.282264	0.282353	0.282304	0.282473	0.282276
Error	0.000004	0.000004	0.000004	0.000005	0.000006	0.000006	0.000005	0.000009	0.000006
ε Hf	−24.23	−22.37	−17.73	−15.42	−17.96	−14.80	−16.54	−10.57	−17.55
$^{176}Hf/^{177}Hf_{initial}$	0.282078	0.282130	0.281748	0.281814	0.281836	0.282015	0.281946	0.281957	0.281925
ε $Hf_{initial}$	+11.01	+12.89	−0.67	+1.64	+2.43	+8.81	+6.33	+6.74	+5.60
Hf T (DM)	1.61	1.54	2.43	2.27	2.14	1.74	1.88	1.91	1.91

Due to analytical problems, lutetium concentration of sample A4A was taken from Table 2. Initial $^{176}Hf/^{177}Hf$ values and ε Hf values were recalculated using the present-day CHUR values of 0.282785 for $^{176}Hf/^{177}Hf$ and 0.0336 for $^{176}Lu/^{177}Hf$ (Bouvier et al. 2008) and the ^{176}Lu decay constant provided by Scherer et al. (2001)

no Pb data are available from the 2.6- to 2.0-Ga-old gneisses from the Kaokoveld (Seth et al. 2002), their Nd isotope composition together with the Nd–Pb isotope data from the leucogranites can be used to place some constraints on the Pb isotope composition of the contaminant. In Fig. 8, the samples define a straight line in ε_{Nd} versus $^{206}Pb/^{204}Pb$ or $^{207}Pb/^{204}Pb$, indicating that the contaminant must have had more negative ε_{Nd} values and more radiogenic $^{206}Pb/^{204}Pb$ and $^{207}Pb/^{204}Pb$ ratios at 1.6 Ga. Recalculating the ε_{Nd} values of the Archaen and Paleoproterozoic gneisses to 1.6 Ga yields an average ε_{Nd} value of −12 (−2.3/± 1.6). At $\varepsilon Nd = -12$, the corresponding $^{206}Pb/^{204}Pb$ and $^{207}Pb/^{204}Pb$ ratios are c. 22 and 16.05, respectively. In $^{206}Pb/^{204}Pb$ versus $^{207}Pb/^{204}Pb$ (Fig. 8), this isotope composition plots very close to the extrapolated best fit straight line defined by the granite feldspar data, again strengthening the role of AFC processes.

Alternatively, the isotope compositions of the samples with negative ε_{Nd} values and moderate radiogenic $^{87}Sr/^{86}Sr$ isotope compositions may have been the result of two-component mixing processes. Some studies (Patchett and Bridgwater 1984; Chauvel et al. 1987) have used simple two-component mixing models to provide constraints on the proportions of juvenile and more evolved crustal components in complex crustal environments. In a two-component mixing model, estimates of juvenile and evolved proportions can be modeled with success when element concentrations and isotope compositions of all end members (primitive magma, contaminated magma, and contaminant) are known. Online Resource 6 shows the result of such model calculations. Using sample A4B as the inferred juvenile end member, sample 8A from Seth et al. (2002) as the contaminant and sample A5 as the contaminated magma, calculated proportions of crustal material are 67% for Nd and 23% for Sr. These values differ significantly and are therefore considered to be unrealistic. This can be taken as evidence that complex melting-assimilation-storage-homogenization models (the MASH model of Hildreth and Moorbath 1988) were not operative. Long-lived and complex zones of interaction in the lower crust where juvenile magmas and crustal derivatives mix until buoyant ascent of magmas is possible were probably not established. Ignoring the variation in $^{87}Sr/^{86}Sr$ because of the large uncertainty that may result from the high $^{87}Rb/^{86}Sr$ ratios, the calculations show that although some of the granites clearly contain a crustal signature, they are probably dominated by a juvenile component.

Compositional controls on the source of the granites

Geochemical criteria that precisely define the source of these leucogranites are difficult to establish. In general,

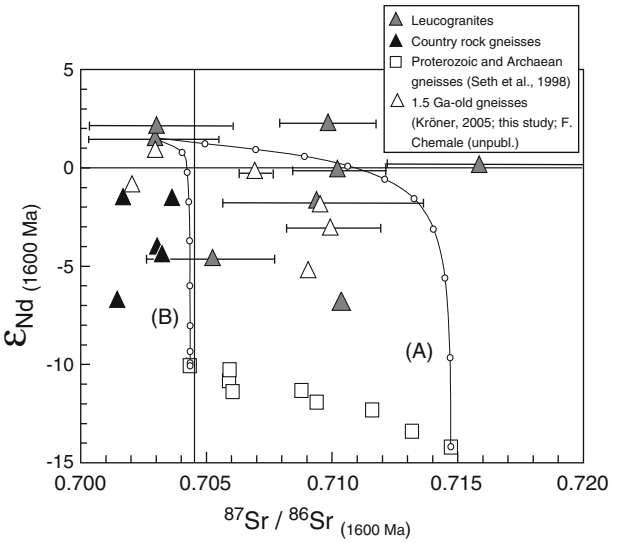

Fig. 5 Initial ε_{Nd} versus initial $^{87}Sr/^{86}Sr$ diagram for leucogranites and country rock gneisses. Archaen to Proterozoic basement is taken from Seth et al. (2002). *Error bars* for the $^{87}Sr/^{86}Sr$ ratio of the leucogranites are shown assuming an error of 1% for the $^{87}Rb/^{86}Sr$ ratios. *Error bars* for samples with $^{87}Rb/^{86}Sr < 0.5$ are smaller or equal to the symbol size and are omitted for clarity. AFC calculations (DePaolo 1981c) using initial ε_{Nd} vs. $^{87}Sr/^{86}Sr$ ratios of the leucogranites and country rock gneisses are also shown. Assimilation (path A) is best modeled with a parental leucogranite melt (sample A4A) with 92.35 ppm Nd ($^{143}Nd/^{144}Nd$: 0.510645, $\varepsilon_{Nd\ (1,600\ Ma)}$: +1.5), 72 ppm Sr ($^{87}Sr/^{86}Sr_{\ (1,600\ Ma)}$: 0.70296). The contaminant (Archaen gneiss 29A from Seth et al., 2002) has 44 ppm Nd ($^{143}Nd/^{144}Nd$: 0.509843, $\varepsilon_{Nd\ (1,600\ Ma)}$: −14.2), 480 ppm Sr ($^{87}Sr/^{86}Sr_{\ (1,600\ Ma)}$: 0.71474). The r-value (ratio of assimilation to fractional crystallization) was fixed at 0.3. Kds for Sr and Nd were 3.0 and 2.0. Tick marks represent 10% intervals. Assimilation (path B) is modeled using the same parental leucogranite as aforementioned. The contaminant (Proterozoic country rock gneiss 5A from Seth et al., 2002) has 39 ppm Nd ($^{143}Nd/^{144}Nd$: 0.510054, $\varepsilon_{Nd\ (1,600\ Ma)}$: −10.1) and 1,055 ppm Sr ($^{87}Sr/^{86}Sr_{\ (1,600\ Ma)}$: 0.70435). The *r*-value (ratio of assimilation to fractional crystallization) was fixed at 0.6. Kds used for Sr and Nd are 3.0 and 2.0. *Tick marks* represent 10% intervals. For further discussion, see text

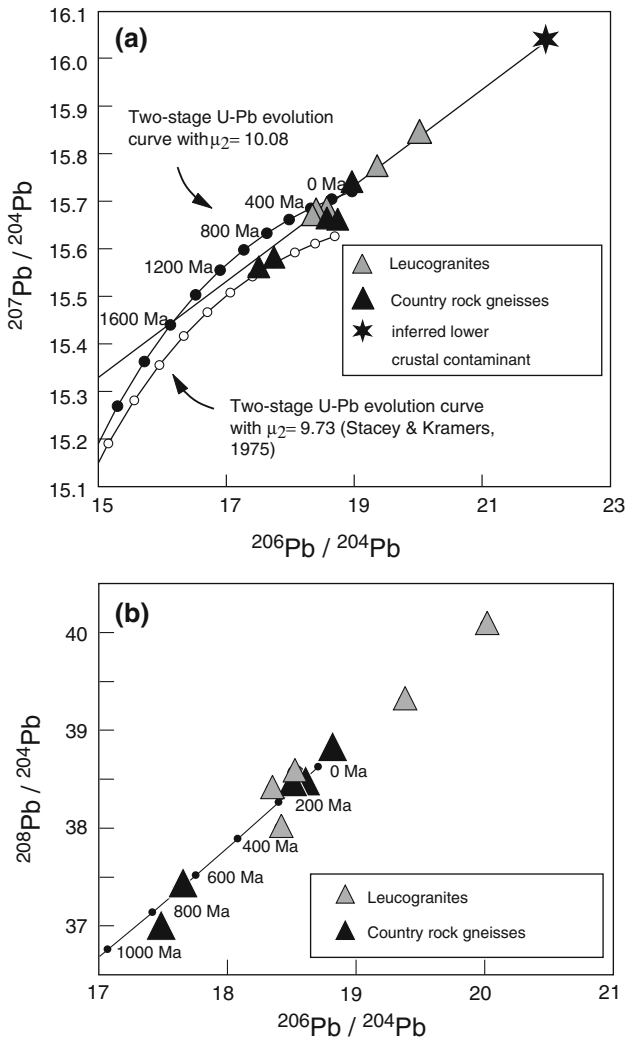

Fig. 6 Plot of **a** $^{207}Pb/^{204}Pb$ and **b** $^{208}Pb/^{204}Pb$ versus $^{206}Pb/^{204}Pb$ isotope ratios of leached K-feldspar for leucogranites and country rock gneisses. The $^{206}Pb/^{204}Pb$ vs. $^{207}Pb/^{204}Pb$ evolution diagram shows the position of the leucogranites relative to a modeled Pb evolution curve using a $\mu = 10.08$ for the second stage. This μ value was chosen to allow the best fit straight line of the leucogranites to intersect the Pb evolution curve at 1.6 Ga. Also shown is the inferred Pb isotope composition of the hypothetical lower crustal contaminant extracted from Fig. 9. In (**b**), the *curve* represents an average Pb growth curve according to Stacey and Kramers (1975) with $\kappa = 4.0$. *Tick marks* represent 200 Ma intervals

some of the geochemical characteristics (enrichment of Ba and Rb relative to Sr, high K_2O, low CaO) of leucogranites indicate a crustal source rock. Based on some major and trace element features (low Na_2O and CaO, high K_2O, moderately high Rb and low Sr), a likely source rock for the leucogranites could be a pelitic metasedimentary rock (Miller 1985; Williamson et al. 1997). However, at rather high SiO_2, high TiO_2, extremely high Ba and high REE abundances and low Al_2O_3 do not support a metapelitic source. Similarly, Sr/Ba ratios are very low (0.05–0.10, excluding two highly fractionated samples), which is not indicative of granitic melts that were generated under water-undersaturated conditions by biotite-dehydration melting from metapelitic sources (Sr/Ba: 0.2–0.7; Harris and Inger 1992). In addition, the Sr and Nd isotope systematics of the inferred unmodified granites with positive ε_{Nd} values and unradiogenic $^{87}Sr/^{86}Sr$ ratios are also not indicative of an evolved metasedimentary source. Therefore, it seems likely that the source of the granite is a meta-igneous protolith. Based on fractionation-corrected depleted mantle Nd model ages (Millisenda et al. 1994) of the granites that range from 1.7 to 1.9 Ga, emplacement ages of the inferred meta-igneous precursor rock cannot be very much older than the granite-forming event. As shown before, the least contaminated leucogranites have Nd isotope characteristics ($\varepsilon Nd_{(1,600\ Ma)} = +2.2$ to +2.3) that

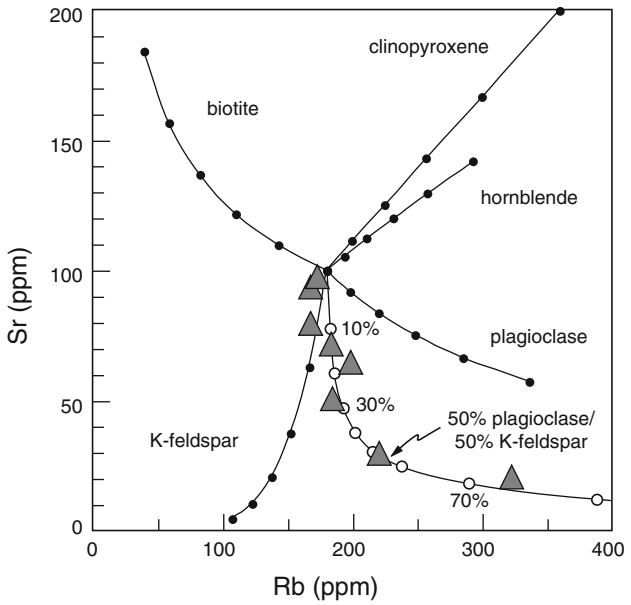

Fig. 7 Variation in Rb versus Sr concentration within the leucogranites. Mineral vectors calculated according to partition coefficients compiled by Rollinson (1993). Compositional trend of the granites indicate 50% crystallization of a 1:1 mixture of K-feldspar and plagioclase. *Dots* represent 10% increments of the fractionating mineral

point to a source less depleted than the depleted mantle at 1.6 Ga with $\varepsilon Nd_{1,600} = +4.1$ (calculated according to Michard et al. (1985) with $^{147}Sm/^{144}Nd = 0.222$ and $^{143}Nd/^{144}Nd = 0.513144$). The two samples that evolved toward lower $^{87}Sr/^{86}Sr$ ratios, negative ε_{Nd} and more radiogenic Pb isotope ratios have slightly older Nd model ages of 1.9 and 2.1 Ga, supporting the view of inheritance of older material. The tightest constraints on the nature of the source material are provided by the Hf isotope data of the zircons which reveal strongly positive ε_{Hf} values of +11 and +13 at 1.6 Ga, again signifying the existence of depleted source material. There is, however, the possibility that metamorphic monazite or apatite overgrown on zircon during the Pan-African metamorphic episode has biased the Hf isotopic composition of the zircons toward more radiogenic values during bulk dissolution. However, significant quantities of monazite or apatite overgrown on zircon can easily be identified during the separation process, and such overgrowth relationships were not observed. Very little is known about the Hf isotopic composition of monazite, but based on its LREE-enriched composition, monazite can be expected to show unradiogenic Hf isotopic compositions coupled with several order of magnitude lower concentrations of Hf relative to zircon. The same applies to apatite with the exception that apatite may show highly variable Lu/Hf ratios and sometimes radiogenic Hf isotope compositions (Barfod et al. 2005; Larsson and Söderlund 2005). Hence, any overgrown monazite will bias the radiogenic Hf isotope composition of the investigated zircons toward more unradiogenic values and cannot lead to radiogenic Hf isotope values as it is observed here. The same applies for apatite, but in the case of radiogenic apatite, due to the lower Hf abundances in apatite relative to zircon, large quantities of apatite are probably needed to significantly bias the Hf isotope composition of zircon. It is therefore more likely that the Hf isotope composition of the early crystallizing zircons mirror that of the melt at the time of melting. During intrusion, the melt was contaminated by older material, thus leading to more unradiogenic Hf isotope composition of the melt. Zircon was unaffected by this process preserving the initial radiogenic Hf isotope

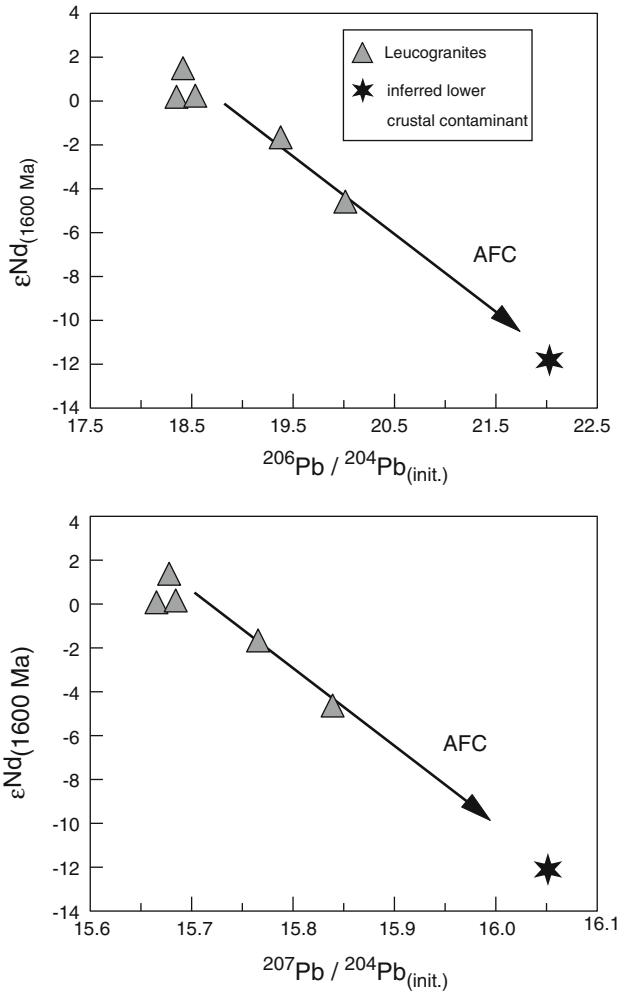

Fig. 8 ε_{Nd} versus Pb isotopes. ε Nd values were determined on whole rock splits and were age-corrected using a U–Pb zircon age of 1.6 Ga. Pb isotopes were determined on hand-picked, acid-leached feldspar separates. Based on the high Pb but negligible U contents of feldspar, no age correction is necessary, and the ratios are assumed to represent initial isotope values. The linear correlation of the leucogranites point to AFC processes of Archaen or Proterozoic lower crustal rocks which have, on average, ε Nd values of c. −12 at 1.6 Ga (Seth et al. 2002). The extrapolation allows the determination of the Pb isotope composition of the Archaen or Proterozoic lower crustal rocks

composition. The view that zircon was an early crystallizing phase is also supported by the high zircon saturation temperatures.

Besides the Hf isotope data of the zircon fractions, the Nd isotope data provide also tight constraints on the nature of the parental reservoirs involved in the generation of the granites. A major contribution from a depleted mantle source seems evident from the positive ε_{Nd} values of the inferred unmodified samples and the positive ε_{Hf} values of the zircons. However, LREE-depleted mafic rocks with early Proterozoic or even Archaen ages have not been reported from the terrane. Basaltic source rocks are often not preserved, because the density of mafic melts favors underplating at the base of the continental crust rather than eruption (Herzberg et al. 1983). Extreme fractionation from a basaltic parent seems therefore unlikely, and an intermediate source rock (i.e., granodiorite to tonalite) that differentiated from a more mafic rock and partly melted shortly before the granite-producing event seems to be a more appropriate source. Therefore, a mafic to intermediate, depleted mantle-derived component may have been introduced slightly before the time of granite genesis, probably in the form of a deep-seated syntectonic intrusion. Extreme models can be ruled out, i.e., remelting of much older ($\gg$ 2.0 Ga) mature crust or crust-derived meta-sedimentary rocks and massive inputs from enriched mantle sources.

A diagram that illustrates mixing and fractionation processes in the Sm–Nd system is presented in Fig. 9, where initial ε_{Nd} values are plotted versus f Sm/Nd which is an expression of the Sm/Nd ratio of the rock. f Sm/Nd is the enrichment factor of $^{147}Sm/^{144}Nd$ in a sample relative to CHUR (DePaolo and Wasserburg 1976). The f Sm/Nd vs. ε_{Nd} plot is useful because normalization of the ratios relative to CHUR magnifies differences between individual rocks and yields a configuration applicable to crustal melting or mantle heterogeneity (Shirey and Hanson 1986). The Archaen to Proterozoic gneisses and the country rock gneisses from this study plot within the quadrant defined by LREE enrichment (negative f Sm/Nd) and time-averaged enrichment (negative ε_{Nd} values). In contrast to the Archaen to Proterozoic gneisses which define a positive correlation, the country rock gneisses show a negative correlation between the two parameters. Most of the granites plot in the quadrant that is characterized by LREE enrichment (negative f Sm/Nd) and time-averaged depletion (positive ε_{Nd} values) with a negative correlation between the two parameters. Mixing relationships, being either mixing of magmas or assimilation processes, yield linear arrays that can have either positive or negative slopes. The country rock gneisses and the leucogranites can be interpreted in this way. The precursor rocks of the country rock gneisses were derived by partial melting of a mantle source with approximately chondritic Nd isotope systematics. Subsequently, these rocks evolved through fractional crystallization toward LREE-enriched compositions indicated by their negative f Sm/Nd values but have probably also assimilated material similar to the least evolved Archaen to Proterozoic gneisses. The leucogranites were derived by partial melting of sources characterized by time averaged LREE depletion (positive ε_{Nd} values) and evolved through fractional crystallization processes toward compositions characterized by LREE enrichment. In addition, assimilation of ancient material was important as it is shown by their negative correlation between f Sm/Nd and ε_{Nd}. This conclusion is also supported by four samples analyzed by Kröner (2005) with U–Pb zircon ages between 1.45 and 1.51 Ga and by three samples analyzed by Luft et al. (2011) with U–Pb ages between 1,503 $\pm$ 12 and 1,506 $\pm$ 19 Ma. It is very likely that these samples correspond to the same igneous suite although five of these samples were collected outside the area under investigation. Note that reworking of pre-existing crust was not important, because in this case, the array defined by the leucogranites should have a positive slope extending from positive ε_{Nd} and negative f Sm/Nd values toward the lower left quadrant with negative ε_{Nd} and negative f Sm/Nd values.

The importance of assimilation of ancient material can also be illustrated using ε_{Hf} vs. ε_{Nd} systematics. It has been shown that the overwhelming majority of mantle and upper crustal lithologies examined thus far lie along a single, well-correlated $^{176}Hf/^{177}Hf$ vs. $^{143}Nd/^{144}Nd$ array. This includes MORBs, OIBs, IAVs, and continental crust of a wide range of lithologies, Achaean to recent, indicating that Lu/Hf and Sm/Nd fractionate in a similar fashion in all terrestrial reservoirs (Vervoort and Patchett 1996; Vervoort et al. 2000 and references therein). It has also been suggested that if garnet is residual from melting or differentiation events, it will impart an elevated Lu/Hf ratio on the bulk rock due to the very high partition coefficients of garnet for Lu compared with Hf. Such high Lu/Hf ratios have been reported for some garnet-bearing granulite facies xenoliths from Kilbourne Hole, New Mexico (Scherer et al. 1997). If the lower crust contains widespread residual or cumulate garnet, "it might develop" decoupled Hf–Nd isotope compositions that will evolve away from the terrestrial Hf–Nd array and should be recognizable in magmas derived from or interacted with, such lower crust. In Fig. 10, ε_{Hf} versus ε_{Nd} isotope systematics of the leucogranites from this study together with unpublished data from the Neoproterozoic Damara orogen are plotted. The Damaran samples show a trend away from the terrestrial ε_{Hf} versus ε_{Nd} array at negative ε_{Hf} and ε_{Nd} values, suggesting derivation from, or interaction with, a lower crust with a slightly elevated Lu/Hf ratio. The leucogranites

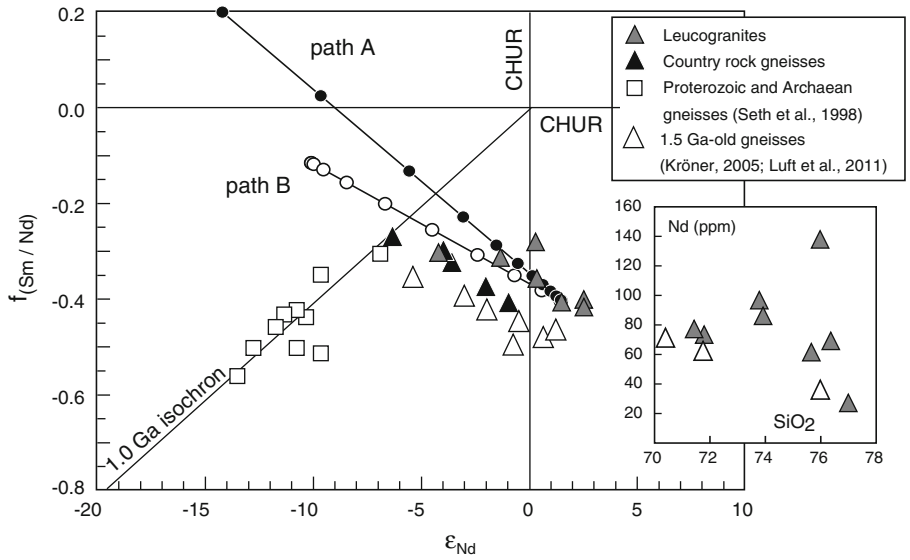

Fig. 9 *f* Sm/Nd versus ε_{Nd} plot for basement rocks, country rock gneisses, and leucogranites from the CKZ, Kaoko Belt (Namibia). All Palaeoproterozoic and Archaen gneisses (Seth et al. 1998), irrespective of their zircon age, plot along an errorchron corresponding to an age of ca. 2.6 Ga in a $^{147}Sm/^{144}Nd$ vs. $^{143}Nd/^{144}Nd$ diagram (not shown in detail). This is suggestive that the 2.0-Ga U–Pb zircon ages of some gneisses (Seth et al. 1998) represent probably a metamorphic age rather than a primary crystallization age of the gneisses. It is further suggestive that the basement gneisses evolved from a common chondritic reservoir at 2.6 Ga (oldest age so far reported from the Kaoko Belt) until ca. 1.6 Ga (inferred age of intrusion of the granites), which is shown by the 1.0 Ga (secondary) isochron. Linear arrays with negative slopes can be interpreted as mixing lines resulting from contamination or AFC processes. Also shown are AFC lines (DePaolo 1981c) with 10% increments originating from inferred uncontaminated granite (sample A4A with 92.35 ppm Nd and 17.84 ppm Sm; ε_{Nd}: +1.5). Contaminants are two of the Archaen (sample BK 29a with 44 ppm Nd and 10 ppm Sm, ε_{Nd} : −14.2; path A) to Proterozoic gneisses (sample BK 5a with 39 ppm Nd and 8.4 ppm Sm; ε_{Nd}: −10.1; path B) taken from Seth et al. (1998). To visualize two different AFC paths, bulk Kds for Sm and Nd are 1.5 and 2.0 (path A) and 1.6 and 2.0 (path B), respectively. The paths end at less negative or even positive *f* Sm/Nd values due to fractionation of monazite or allanite during AFC processes. That monazite or allanite plays a role during fractionation is shown in the inset where the most evolved samples show decreasing Nd concentrations with increasing SiO_2 concentrations. For further explanation, see text

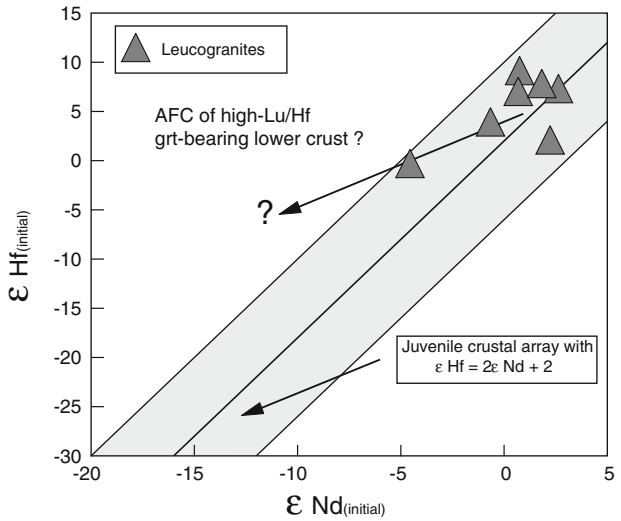

Fig. 10 ε_{Nd} versus ε_{Hf} diagram with initial isotope ratios at 1.6 Ga showing the position of the leucogranites from this study. Interaction with high Lu–Hf lower crust is indicated. Juvenile crustal array together with a ± 8 ε units uncertainty (*shaded area*) is from Vervoort and Patchett (1996)

from this study seem to follow a similar trend and indicate interaction with a lower crustal source with ε_{Nd} of c. −12 (see above) and ε_{Hf} of c. −5 at 1.6 Ga.

Implications from accessory mineral saturation temperatures

Estimates of the conditions of formation and evolution of granites may be obtained from zircon saturation temperatures (Watson and Harrison 1983). Temperatures calculated with this geothermometer are based on the assumption that the rocks do not contain restitic zircon, which, in our case, is supported by LA-ICP-MS studies that did not reveal any inherited core material and zircon is an early crystallising phase. Consistent results can only be expected if (1) chemical equilibrium prevailed during melting or crystallisation, (2) zircon was not present as inclusion in residual minerals, and (3) the whole rock composition approximates a frozen melt. These assumptions are difficult to test. In Table 2, calculated zircon saturation temperatures are given, and for the samples with positive ε_{Nd} values, temperatures are >920°C. These temperatures correlate with initial ε_{Nd} values as a measure of

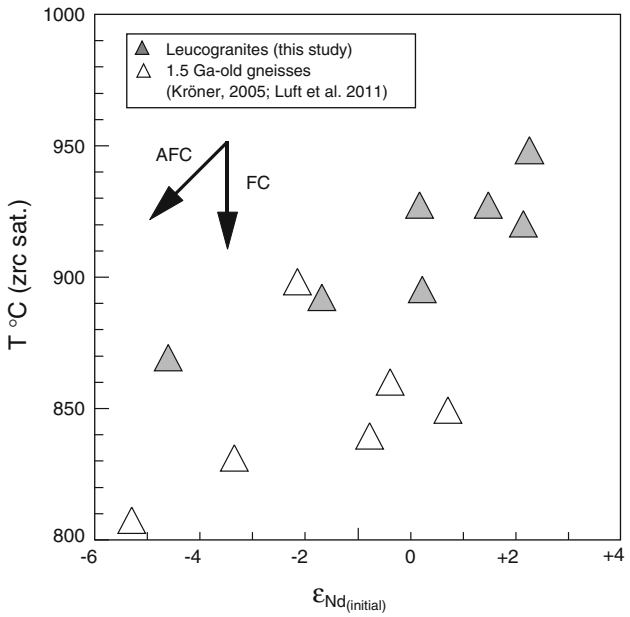

Fig. 11 Zircon saturation temperature versus ε_{Nd} value for leucogranites from this study and 1.5-Ga-old granites taken from Kröner (2005) and Luft et al. (2011). Decreasing zircon saturation temperatures with decreasing ε_{Nd} values indicate AFC (assimilation-fractional crystallization) processes. Lower zircon saturation temperatures at comparatively radiogenic ε_{Nd} values suggest the predominance of FC (fractional crystallization) processes in the early stages of the evolution

AFC processes (Fig. 11), in which the most fractionated and presumably most contaminated sample still records a Zr saturation temperature of c. 870°C. This implies that the parental melts were even hotter and support the argument that the samples with positive ε_{Nd} values contain a significant mantle component.

Concluding remarks

This study shows that Mesoproterozoic leucogranites from the high-grade Kaoko Belt in Namibia are broadly similar in their major element chemistry but can have distinct trace element and Sr and Nd isotope characteristics. These features are most likely the result of AFC processes in the deep crust. The recognition of isotope patterns suggestive of anatexis of mantle-derived igneous rocks with short crustal residence times followed by interaction with crustal rocks provides an alternative to previous models that favor anatexis of depleted granulite facies rocks. In our view, there is no requirement for the mantle-derived end member to be a single-stage product of the subcrustal mantle. It may have undergone significant fractionation at the base of the crust or, in a complex environment of magmatic underplating, intermediate material added to the crust may have been remelted. In addition, the inferred high temperatures from the application of zircon saturation thermometry in excess of 900°C could be related to the temperature of the mantle-derived magma flux. Primitive magmas with high liquidus temperatures have substantial capacities to assimilate and thermally interact with crustal rocks as a consequence of the large energy released by olivine and clinopyroxene crystallization (Sparks 1986). Since magmas similar to the granites observed here are commonly generated in post-collisional settings, lithospheric delamination following continental collision provides a likely mechanism for upwelling and melting of material from deeper levels in the mantle (Sachs and Secor 1990). The high heat flow and massive thermal transfer from the crystallization of a primitive magma would provide the necessary conditions for developing a high-temperature, restite-free, H_2O-undersaturated granite magma. Considering the isotope composition of the samples with positive ε_{Nd} values, a simple explanation is that the parental sources of the granites represent juvenile material with characteristics of the depleted mantle. Proterozoic igneous rocks, emplaced shortly before the granite-forming event, had only a short residence time and thus would exert far less isotopic leverage than the Archaen rocks to serve as possible sources. Such isotopically primitive rocks of Proterozoic age have not been described from the currently exposed parts of the Kaoko Belt. Since the precursor rocks of the granites must have had only a very short crustal residence time, intrusion of such material mark an episode of crustal growth in the Proterozoic of Africa during which some mantle material was added to the crust.

Acknowledgments The Sr, Nd, and Pb isotope analyses were supported by the Max-Planck-Society, and Albrecht W. Hofmann (Max-Planck-Institut, Mainz) is thanked for hospitality and free access to mass spectrometry facilities while Stefan Jung held a postdoc position in Mainz. Iris Bambach (Max-Planck-Institut, Mainz) did a superb job in managing the line drawings. Andreas Busch (Marburg) is thanked for providing major and trace element data. Stefan Jung acknowledges the help of Alfred Kröner in providing sample material from the PhD study of Stephan Kröner. Farid Chemale Jr. (University of Brasil; Brasilia) is warmly thanked for giving access to unpublished Sr isotope data. We would like to thank J. Patchett and an anonymous reviewer for very constructive reviews that greatly improved the manuscript. We also appreciate the patient and professional editorial handling of the manuscript by Jochen Hoefs.

References

Ayuso RA, Bevier ML (1991) Regional differences in Pb isotopic compositions of feldspars in plutonic rocks of the northern Appalachian mountains, USA and Canada: a geochemical method of terrane correlation. Tectonics 10:191–212

Barfod GH, Krogstad EJ, Frei R, Albarède F (2005) Lu-Hf and PbSL geochronology of apatites from Proterozoic terranes: a first look at Lu-Hf isotopic closure in metamorphic apatite. Geochim Cosmochim Acta 69:1847–1859

Ben Othman D, Fourcade S, Allègre CJ (1984) Recycling processes in granite-granodiorite complex genesis: the Quérigut case studied by Nd-Sr isotope systematics. Earth Planet Sci Lett 69:290–300

Bennett VC, DePaolo DJ (1987) Proterozoic crustal history of the western United States as determined by neodymium isotopic mapping. Geol Soc Am Bull 99:674–685

Bernard-Griffiths J, Peucat JJ, Sheppard S, Vidal P (1985) Petrogenesis of Hercynian leucogranites from the southern Armorican Massif: contribution of REE and isotopic (Sr, Nd, Pb, O) geochemical data to the study of source rock characteristics and ages. Earth Planet Sci Lett 74:235–250

Bleiner D, Günther D (2001) Theoretical description and experimental observation of aerosol transport processes in laser ablation inductively coupled plasma mass spectrometry. J Anal At Spectrom 16:449–456

Blichert-Toft J, Chauvel C, Albarède F (1997) Separation of Hf and Lu for high-precision isotope analysis of rock samples by magnetic sector-multiple collector ICP-MS. Contrib Mineral Petrol 127:248–260

Bouvier A, Vervoort JD, Patchett PJ (2008) The Lu–Hf and Sm–Nd isotopic composition of CHUR: constraints from unequilibrated chondrites and implications for the bulk composition of terrestrial planets. Earth Planet Sci Lett 273:48–57

Boynton WV (1984) Geochemistry of rare earth elements: Meteorite studies. In: Henderson P (ed) Rare earth element geochemistry. Elsevier, New York, pp 63–114

Brandt S, Will TM, Klemd R (2007) Ultrahigh-temperature metamorphism and anticlockwise PT paths of sapphirine-bearing orthopyroxene-sillimanite gneisses from the Proterozoic Epupa Complex, NW Namibia. Prec Res 153:143–178

Cameron AE, Smith DH, Walker RL (1969) Mass spectrometry of nanogram-size samples of lead. Anal Chem 41:525–526

Chauvel C, Arndt NT, Keilinzcuk S, Thom A (1987) Formation of Canadian 1.9 Ga old continental crust. 1. Nd isotope data. Can J Earth Sci 24:396–406

Crawford MB, Windley BF (1990) Leucogranites of the Himalaya/Karakoam: implications for magmatic evolution within collisional belts and the study of collision-related leucogranite petrogenesis. J Volc Geotherm Res 44:1–19

Deniel C, Vidal P, Fernadez A, LeFort P, Peucat J-J (1987) Isotopic study of the Manaslu granite (Himalaya; Nepal): inferences on the age and source of Himalayan leucogranites. Contrib Mineral Petrol 96:78–92

DePaolo DJ (1981a) Neodymium isotopes in the Colorado front range and crust-mantle evolution in the Proterozoic. Nature 291:193–196

DePaolo DJ (1981b) A neodymium and strontium study of the Mesozoic calc-alkaline granitic batholiths of the Sierra Nevada and Peninsula Ranges, California. J Geophys Res 86:10470–10488

DePaolo DJ (1981c) Trace elements and isotopic effects of combined wallrock assimilation and fractional crystallization. Earth Planet Sci Lett 53:189–202

DePaolo DJ, Wasserburg GJ (1976) Nd isotopic variations and petrogenetic models. Geophys Res Lett 3:249–252

Dietrich V, Gansser A (1981) The leucogranites of the Bhutan Himalaya (crustal anatexis versus mantle melting). Schweiz Miner Petrogr Mitt 61:177–202

Dorais MJ, Paige ML (2000) Regional geochemical and isotopic variations of northern New England plutons: implications for magma sources and for Grenville and Avalon basement-terrane boundaries. Geol Soc Am Bull 112:900–914

Drüppel K, Littmann S, Romer RL, Okrusch M (2007) Petrology and isotope geochemistry of the Mesoproterozoic anorthosite and related rocks of the Kunene Intrusive Complex, NW Namibia. Prec Res 156:1–31

Dürr SB, Dingeldey DP (1996) The Kaoko belt (Namibia): part of a late Neoproterozoic continental-scale strike-slip system. Geology 24:503–506

France-Lanord C, Le Fort P (1988) Crustal melting and granite genesis during the Himalayan collision orogenesis. Trans Roy Soc Edinburgh Earth Sci 79:183–195

Franz L, Romer R, Dingeldey DP (1999) Diachronous Pan-African granulite-facies metamorphism (650 and 550 Ma) in the Kaoko Belt, NW Namibia. Eur J Mineral 11:167–180

Goscombe B, Hand M, Gray D, Mawby J (2003) The metamorphic architecture of a transpressional orogen: the Kaoko Belt, Namibia. J Petrol 44:679–711

Halliday AN, Stephens WE, Harmon RS (1980) Rb-Sr and O isotope relationships in 3 zoned Caledonian granitic plutons, Southern Uplands, Scotland: evidence for varied sources and hybridisation of magmas. J Geol Soc London 137:329–348

Harris NBW, Inger S (1992) Trace element modelling of pelite derived granites. Contrib Mineral Petrol 110:46–56

Heinrichs H, Herrmann AG (1990) Praktikum der Analytischen Geochemie. Springer, Berlin

Herzberg CT, Fyfe WS, Carr MJ (1983) Density constraints on the formation of the continental Moho and crust. Contrib Mineral Petrol 84:1–5

Hildreth EW, Moorbath S (1988) Crustal contribution to arc magmatism in the Andes of central Chile. Contrib Mineral Petrol 98:455–489

Inger S, Harris N (1993) Geochemical constraints on leucogranite magmatism in the Langtang Valeey, Nepal Himalaya. J Petrol 34:345–368

Jackson S, Pearson NJ, Griffin WL, Belousova EA (2004) The application of laser ablation-inductively coupled plasma-mass spectrometry to in situ U-Pb zircon geochronology. Chem Geol 211:47–69

Jacobsen SB, Wasserburg GJ (1980) Sm-Nd isotopic evolution of chondrites. Earth Planet Sci Lett 50:139–155

Jung S, Hoernes S, Hoffer E (2005) Petrogenesis of cogenetic nepheline and quartz syenites and granites (Northern Damara orogen, Namibia)—enriched mantle vs. crustal contamination. J Geol 113:651–672

Kerr A, Fryer BJ (1993) Nd isotope evidence for crust-mantle interaction in the generation of A-type granitoid suites in Labrador, Canada. Chem Geol 104:39–60

Konopásek J, Kröner S, Kitt SL, Passchier CW, Kröner A (2005) Oblique collision and evolution of large-scale transcurrent shear zones in the Kaoko belt, NW Namibia. Prec Res 136:139–157

Kröner S (2005) Geochronological and structural evolution of the western and central Kaoko Belt in NW Namibia. Dissertation, University of Mainz

Kröner S, Konopásek J, Kröner A, Passchier CW, Poller U, Wingate MTD, Hofmann KH (2004) U-Pb and Pb-Pb zircon ages for metamorphic rocks in the Kaoko Belt of Northwestern Namibia: A Palaeo- to Mesoproterozoic basement reworked during the Pan-African orogeny. S Afr J Geol 107:455–476

Larsson D, Söderlund U (2005) Lu-Hf apatite geochronology of mafic cumulates: an example from a Fe–Ti mineralization at Smalands Taberg, southern Sweden. Chem Geol 224:201–211

Lechler PJ, Desilets MO (1987) A review of the use of loss on ignition as a measurement of total volatiles in whole rock analysis. Chem Geol 63:341–344

LeFort P, Cuney M, Deniel C, France-Lanord C, Sheppard SMF, Upreti BN, Vidal P (1987) Crustal generation of the Himalayan leucogranites. Tectonophysics 134:39–57

Luft JL Jr, Chemale F Jr, Armstrong R (2011) Evidence of 1.7 to 1.8 Ga-old collisional arc in the Kaoko Belt, NW Namibia. Int J Earth Sci 100:305–321

Mattinson JM (1986) Geochronology of high-pressure-low temperature Franciscan metabasites. A new approach using the U-Pb system. Geol Soc Amer Mem 164:95–105

McCulloch MT, Chappell BW (1982) Nd isotope characteristics of S- and I-type granites. Earth Planet Sci Lett 58:51–64
Michard A, Guriet P, Soudant M, Albarède F (1985) Nd isotopes in French Phanerozoic shales: external vs. internal aspects of crustal evolution. Geochim Cosmochim Acta 49:601–610
Miller RMCG (1983) The Pan-African Damara Orogen of Namibia. In: Miller RMcG (ed) The Damara Orogen. Spec Publ Geol Soc S Afr, vol 11, pp 431–515
Miller CF (1985) Are strongly peraluminous magmas derived from pelitic sedimentary sources? J Geol 93:673–689
Miller RMCG (2008) The geology of Namibia, vol 1 Archean to Mesoproterozoic. Ministry of Mines and Energy, Geological Survey, Windhoek, p 320
Millisenda C, Liew TC, Hofmann AW, Köhler H (1994) Nd isotopic mapping of the Sri Lanka basement: updata, and additional constraints from Sr isotopes. Prec Res 66:95–110
Morel MLA, Nebel O, Nebel-Jacobsen Y, Miller JS, Vroon PZ (2008) Hafnium isotope characterization of the GJ-1 zircon reference material by solution and laser-ablation MC-ICPMS. Chem Geol 255:231–235
Münker C, Weyer S, Scherer EE, Mezger K (2001) Separation of High Field Strength Elements (Nb, Ta, Zr, Hf, and Lu) from rock samples for MC-ICPMS measurements. Geochem Geophys Geosys 2:2002GC000183
Nebel O, Morel MLA, Vroon PZ (2009) Isotope dilution analyses of Lu, Hf, Zr, Ta and W, and Hf-isotope compositions of NIST SRM-610 and SRM-612 glass wafers. Geostandard Geoanalytical Res 33:487–499
Nebel O, van Westrenen W, Vroon PZ, Wille M, Raith MM (2010a) Deep mantle storage of the Earth's missing niobium in late-stage residual melts from a Hadean magma ocean. Geochim Cosmochim Acta 74:4392–4404
Nebel O, Vroon PZ, Wiggers de Vries DF, Jenner F, Mavrogenes JA (2010b) Tungsten isotopes as tracers of core—mantle interactions: the influence of subducted sediments. Geochim Cosmochim Acta 74:751–762
Nebel-Jacobsen Y, Scherer EE, Münker C, Mezger K (2005) Separation of U, Pb, Lu, and Hf from single zircons for combined U-Pb dating and Hf isotope measurements by TIMS and MC-ICPMS. Chem Geol 220:105–120
Ortega LA, Gil-Ibarguchi JIG (1990) The genesis of late Hercynian granitoids from Galicia (northwestern Spain): Inferences from REE studies. J Geol 98:189–211
Passchier CW, Trouw RAJ, Ribeiro A, Paciullo FVP (2002) Tectonic evolution of the southern Kaoko Belt, Namibia. J Afr Earth Sci 35:61–75
Patchett PJ, Bridgwater D (1984) Origin of continental crust of 1.9–1.7 Ga age defined by Nd isotopes in the Ketilidian terrain of South Greenland. Contrib Mineral Petrol 87:311–318
Pickett DA, Wasserburg GJ (1989) Neodymium and strontium isotope characteristics of New Zealand granitoids and related rocks. Contrib Mineral Petrol 103:131–142
Porada H (1989) Pan-African rifting and orogenesis in southern to equatorial Africa and eastern Brazil. Prec Res 44:103–136
Prave AR (1996) Tale of three cratons: tectonostratigraphic anatomy of the Damara Orogen in northwestern Namibia and the assembly of Gondwana. Geology 24:1115–1118
Pupin JP (1980) Zircon and granite petrology. Contrib Mineral Petrol 73:207–220
Rollinson HR (1993) Using geochemical data: evaluation, presentation, interpretation. Longman/Wiley, London/NJ, p 352
Rudnick RL, Fountain DM (1995) Nature and composition of the continental crust-a lower crustal perspective. Rev Geophys 33:267–309
Sachs PE, Secor DT Jr (1990) Delamination in collisional orogens. Geology 18:999–1002
Scaillet B, France-Lanord C, LeFort P (1990) Badrinath-Gangotri plutons (Gharwal, India): petrological and geochemical evidence for fractionation processes in a high Himalayan leucogranite. J Volc Geotherm Res 44:163–188
Scherer EE, Cameron KL, Johnson CM, Beard BL, Barovich KM, Collerson KD (1997) Lu-Hf geochronology applied to dating Cenozoic events affecting lower crustal xenoliths from Kilbourne Hole, New Mexico. Chem Geol 142:63–78
Scherer EE, Münker C, Mezger K (2001) Calibration of the lutetium-hafnium clock. Science 293:683–687
Searle MP, Crawford MB, Rex AJ (1992) Field relations, geochemistry, origin and emplacement of the Baltoro Granite, central Karakoram. Trans Roy Soc Edinburg Earth Sci 83:519–538
Searle MP, Parrish RR, Hodges KV, Hurford KV, Ayres MW, Whitehouse MJ (1997) Shisha Pangma leucogranite, South Tibetean Himalaya: Field relations, geochemistry, age, origin, and emplacement. J Geol 195:295–317
Seth B, Kröner A, Mezger K, Nemchin AA, Pidgeon RT, Okrusch M (1998) Archaean to Neoproterozoic magmatic events in the Kaoko belt of NW Namibia and their geodynamic significance. Prec Res 92:341–363
Seth B, Okrusch M, Wilde M, Hoffmann KH (2000) The Voetspoer intrusion, southern Kaoko zone, Namibia: mineralogical, geochemical and isotopic constraints for the origin of a syenitic magma. Communs Geol Surv Namibia 12:125–137
Seth B, Jung S, Hoernes S (2002) Isotope constraints on the origin of Pan African granitoid rocks in the Kaoko Belt NW Namibia. South Afr J Geol 105:179–192
Seth B, Jung S, Gruner B (2008) Deciphering polymetamorphic episodes in high-grade metamorphic orogens: Constraints from PbSL, Sm/Nd and Lu/Hf garnet dating of low- to high-grade metasedimentary rocks from the Kaoko belt (Namibia). Lithos 104:131–146
Shirey SB, Hanson GN (1986) Mantle heterogeneity and crustal recycling in Archean granite-greenstone belts: Evidence from Nd isotopes and trace elements in the Rainy Lake area, Superior Province, Ontario, Canada. Geochim Cosmochim Acta 50:2631–2651
Sláma J, Košler J, Condon DJ, Crowley JL, Gerdes A, Hanchar JM, Horstwood MSA, Morris GA, Nasdala L, Norberg N, Schaltegger U, Schoene B, Tubrett MN, Whitehouse MJ (2008) Plešovice zircon—A new natural reference material for U-Pb and Hf isotopic microanalysis. Chem Geol 249:1–35
Sparks RSJ (1986) The role of crustal contamination in magma evolution through geological time. Earth Planet Sci Lett 78:211–223
Stacey JS, Kramers JD (1975) Approximation of terrestrial lead isotope evolution by a two-stage model. Earth Planet Sci Lett 26:207–221
Sylvester PJ, Ghaderi M (1997) Trace element analysis of scheelite by Excimer laser ablation inductively coupled plasma mass spectrometry (ELA-ICP-MS) using a synthetic silicate glass standard. Chem Geol 141:49–65
Trompette R, Carozzi AV (1994) Geology of Western Gondwana (2000–500 Ma). Pan-African–Brasiliano aggregation of South America and Africa. A. A. Balkema, Rotterdam
Vervoort JD, Patchett PJ (1996) Behaviour of hafnium and neodymium isotopes in the crust: constraints from Precambrian crustally derived granites. Geochim Cosmochim Acta 60:3717–3733
Vervoort JD, Patchett PJ, Albarède F, Blichert-Toft J, Rudnick R, Downes H (2000) Hf-Nd isotopic evolution of the lower crust. Earth Planet Sci Lett 181:115–129
Vidal P, Cocherie A, LeFort P (1982) Geochemical investigations of the origin of the Manslu leucogranite (Himalaya, Nepal). Geochim Cosmochim Acta 46:2279–2292

Watson EB, Harrison TM (1983) Zircon saturation revisited: temperature and composition effects in a variety of crustal magma types. Earth Planet Sci Lett 64:295–304

Werner CD (1987) Saxonian granulites—igneous or lithogenous? A contribution to the geochemical diagnosis of the original rocks in high-metamorphic complexes. In: Gerstenberger H (ed) Contribution to the geology of the Saxonian granulite massif (Sächsisches Granulitgebirge). Zfl-Mitteilungen 133:221–250

Will TM, Okrusch M, Gruner BB (2004) Barrovian and Buchan type metamorphism in the Pan-African Kaoko Belt, Namibia: implications for its geotectonic position within the framework of Western Gondwana. S Afr J Geol 107:431–454

Williamson BJ, Downes H, Thirlwall MF, Beard A (1997) Geochemical constraints on restite composition and unmixing in the Velay anatectic granite, French Massif Central. Lithos 40:295–319